Biodegradable Thin Metal Foils and Spin-On Glass Materials for Transient Electronics

*Seung-Kyun Kang, Suk-Won Hwang, Sooyoun Yu, Jung-Hun Seo, Elise A. Corbin, Jiho Shin, Dae Seung Wie, Rashid Bashir, Zhenqiang Ma, and John A. Rogers**

Biodegradable substrates and encapsulating materials play critical roles in the development of an emerging class of semiconductor technology, generally referred as "transient electronics", whose key characteristic is an ability to dissolve completely, in a controlled manner, upon immersion in ground water or biofluids. The results presented here introduce the use of thin foils of Mo, Fe, W, or Zn as biodegradable substrates and silicate spin-on-glass (SOG) materials as insulating and encapsulating layers, with demonstrations of transient active (diode and transistor) and passive (capacitor and inductor) electronic components. Complete measurements of electrical characteristics demonstrate that the device performance can reach levels comparable to those possible with conventional, nontransient materials. Dissolution kinetics of the foils and cytotoxicity tests of the SOG yield information relevant to use in transient electronics for temporary biomedical implants, resorbable environmental monitors, and reduced waste consumer electronics.

1. Introduction

Biodegradable metals and organic polymers are used widely in biomedicine and biomedical research, where they serve as passive implants and drug delivery vehicles that dissolve in the body in a controlled fashion. Although the chemical diversity and easy processability of polymers represent advantages, metals offer superior mechanical properties and they are dimensionally stable, i.e., they do not swell in biofluids. These features of metals are important for applications in biodegradable coronary stents[1] and bone fixation screws/pins.[2,3] Here, we illustrate that these same characteristics make thin metal foils well suited for use as substrates and as parts of encapsulating packages in emerging classes of biodegradable electronics and related semiconductor devices. A successful technology of this type has the potential to dramatically expand the range of functions that are possible in temporary implants. The same concepts enable other unusual applications, such as devices that environmentally resorb to facilitate disposal without separate waste streams or that fully or partly decompose/disintegrate/dissolve to provide hardware-level antitamper functionality.[4–19] High performance biodegradable electronics are enabled by using single crystalline silicon nanomembranes (Si NMs), or other forms of silicon, silicon germanium, or metal oxides (e.g., ZnO) for the semiconductors; MgO, SiO_2, or SiN_x for the gate/interlayer dielectrics; and Mg, Mo, Fe, W, or Zn for the electrodes and interconnects.[4–10] Organic polymers have some value as substrates and encapsulating materials. Demonstrated options include films of silk fibroin,[4,5,7,9,11,12] polycaprolactone (PCL), polyglycolic acid (PGA), polylactic acid (PLA), polylactic-co-glycolic acid (PLGA, a copolymer of PLA and PGA), collagen, and even rice paper.[10] This collective set of materials, together with advanced manufacturing schemes and device designs, provides routes to many types of active and passive electronic components, including resistors, inductors, capacitors, antennas, transistors, and diodes.[4,10–12] Solar cells, mechanical energy harvesters (MEH), strain and temperature sensors, photodetectors, and other devices are also possible.[4,5] System examples include radio frequency (RF) scavenger circuits, complementary metal-oxide-semiconductor (CMOS) ring oscillators, and digital imagers for wireless power, RF communication devices,

Dr. S.-K. Kang, D. S. Wie, Prof. J. A. Rogers
Department of Materials Science and Engineering
Frederick Seitz Materials Research Laboratory
University of Illinois at Urbana-Champaign
Urbana, IL 61801, USA
E-mail: jrogers@illinois.edu

Prof. S.-W. Hwang
KU-KIST Graduate School of Converging Science and Technology
Korea University
Seoul 136-701, Korea

S. Yu, J. Shin
Department of Chemical and Biomolecular Engineering
University of Illinois at Urbana-Champaign
Urbana, IL 61801, USA

Dr. J.-H. Seo, Prof. Z. Ma
Department of Electrical and Computer Engineering
University of Wisconsin-Madison
Madison, WI 53706, USA

Dr. E. A. Corbin, Prof. R. Bashir
Department of Bioengineering
University of Illinois at Urbana-Champaign
Urbana, IL 61801, USA

Prof. J. A. Rogers
Department of Chemistry
Mechanical Science and Engineering,
and Department of Electrical and Computer Engineering
Beckman Institute for Advanced Science and Technology
University of Illinois at Urbana-Champaign
Urbana, IL 61801, USA

DOI: 10.1002/adfm.201403469

© 2015 WILEY-VCH Verlag GmbH & Co. KGaA, Weinheim

and cameras.[4,12] Disadvantages of polymer substrates include their incompatibility with many aspects of semiconductor processing, their tendency to swell in a way that can crack the supported electronic materials when immersed in water or biofluids, their poor thermal stability, and their nonzero water permeability. By contrast, metal foils are robust, capable of providing hermetic protection, compatible with most device fabrication steps, and thermally and chemically stable. The results presented in the following illustrate the utility of molybdenum, iron, tungsten, and zinc foils as substrates and of spin-on glass (SOG) materials as passivating and bonding interlayers for water-soluble forms of transient electronics.

2. Results and Discussion

Figure 1a illustrates a fabrication strategy for transient *n*-channel metal–oxide–semiconductor field effect transistors (MOSFETs) on biodegradable metal foils. Fabrication starts with laminating the foils (Fe, Mo, W, and Zn, ≈10 µm thick; Goodfellow, USA; foils of Mg and Mg alloys can also be considered, although the high costs might prohibit use in many applications) on glass slides coated with poly(dimethylsiloxane) (PDMS, Dow Corning Co., USA) as temporary supports during device processing. A layer of SiO_2 (≈1 µm) deposited by plasma-enhanced chemical vapor deposition (PECVD) on the foils electrically isolates them from the supported device layers. A layer of SOG (Filmtronics, Inc., USA), described in detail subsequently, serves as an adhesive layer for transfer printing Si NMs with patterns of dopants introduced by diffusion of phosphorus from a solid source at 950 °C. Reactive ion etching (RIE, Plasmatherm, USA) with sulfur hexafluoride (SF_6) gas patterns the Si into areas that match the desired device layouts. Photolithographic patterning of materials deposited by PECVD and electron beam (E-beam) evaporation yield gate dielectrics (SiO_2, ≈100 nm) and metal electrodes (Mg, ≈300 nm), respectively. This straightforward type of processing is trivial on metal foils but extremely difficult on biodegradable polymer substrates, due to their limited thermal, mechanical, and chemical stability. Figure 1b shows a Fe foil of thickness ≈10 µm (left; surface topography measured with an atomic force microscope (AFM) on the right) and an array of *n*-channel MOSFETs on this substrate (Figure 1c), respectively. The small thickness of the foil leads naturally to a low bending stiffness which, together with its physical toughness, affords a robust, mechanical flexible support, of importance for many classes of biomedical devices (Figure S1a, Supporting Information).[20] Figure S1b,c, Supporting Information, presents examples of use at elevated temperatures (for applications in certain types

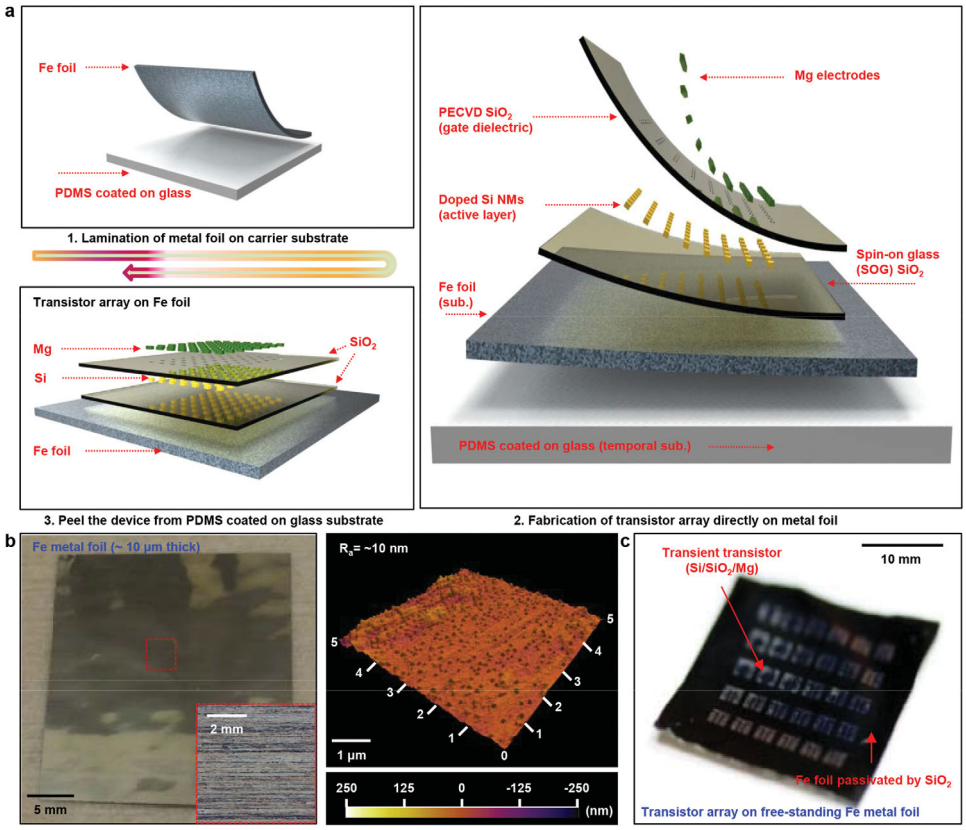

Figure 1. Fabrication procedures for transient *n*-channel metal–oxide–semiconductor field effect transistors (MOSFETs) array on a biodegradable Fe foil. a) Lamination of a Fe foil on a PDMS-coated glass substrate (top left). Exploded-view schematic illustration of a transient *n*-MOSFET (right). Detachment from the PDMS/glass substrate yields a free-standing system (bottom left). The materials include silicon nanomembranes (Si NMs; semiconductor), thin magnesium (conductor) films, spin-on glass (SOG, dielectrics), silicon dioxide (SiO_2, dielectric), and Fe foil (substrate), all of which are biodegradable. b) Image of ≈10 µm thick Fe (left) and microscope image (inset). Surface topography of Fe foils (right) measured with an atomic force microscope (AFM). c) Image of array of *n*-channel MOSFETs fabricated on the Fe foil.

© 2015 WILEY-VCH Verlag GmbH & Co. KGaA, Weinheim
Adv. Funct. Mater. **2015**,
DOI: 10.1002/adfm.201403469

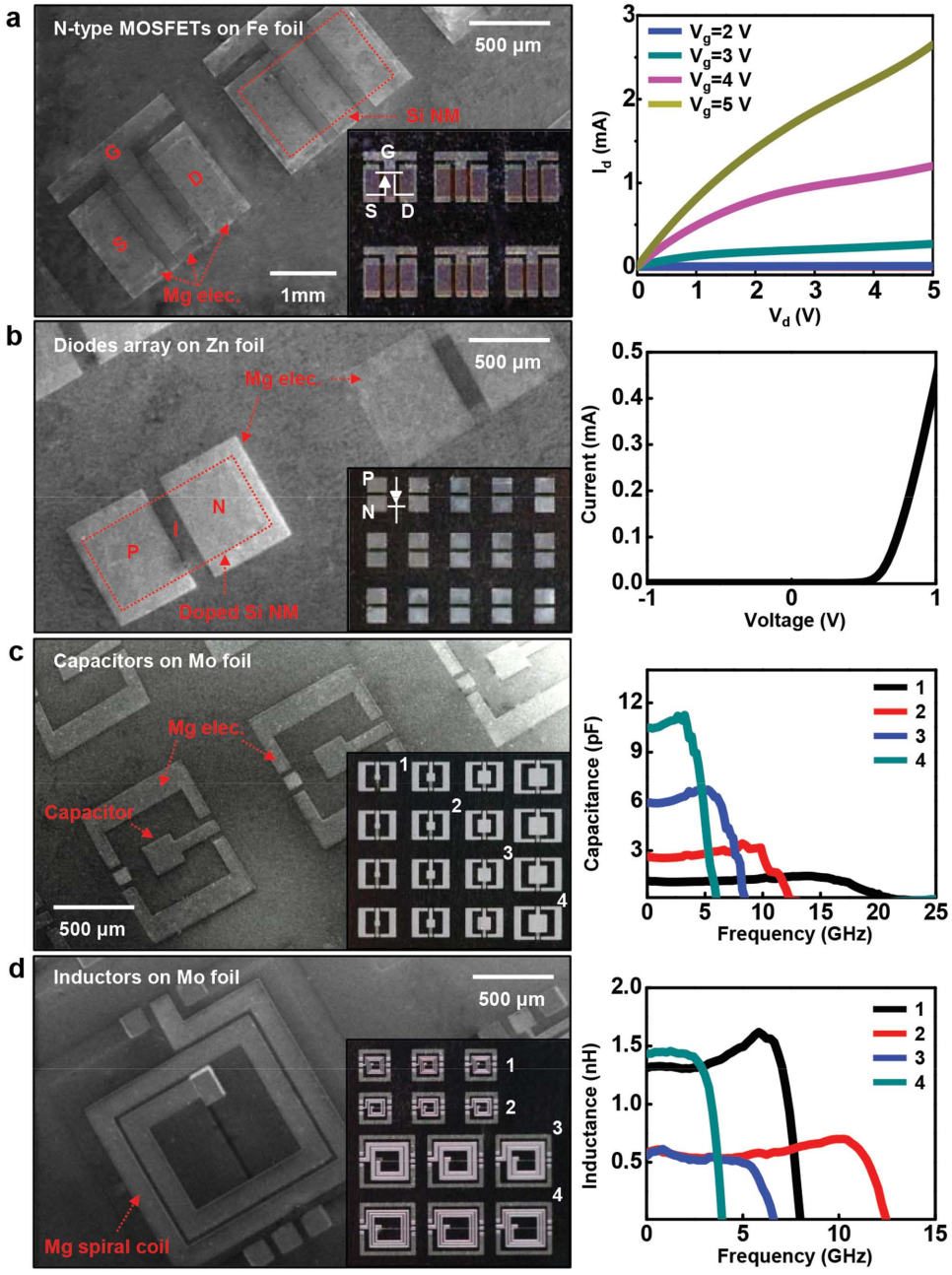

Figure 2. Images and electrical properties of diverse transient electronic devices on various biodegradable metal foil substrates. a) Scanning electron microscope (SEM) and optical microscope image (inset) of an array of *n*-MOSFETs on Fe foil (≈10 μm thick) (left); *I*–*V* characteristics of a representative device (right). The channel length *L* and width *W* are 30 and 600 μm, respectively. The mobility (linear regime) is ≈400 $cm^2 V^{-1} s$. V_g is gate voltage. b) Transient PIN diode on a Zn foil (≈10 μm thick) observed by SEM and optical microscope (left and inset). Current–voltage characteristics are typical of PIN diodes (right). c) SEM and optical images of capacitors with different sizes, built using Mg electrodes (top/bottom) and PECVD SiO_2 dielectrics on Mo foil (≈10 μm thick) (left). Measured capacitance as a function of frequency up to ≈25 GHz. The overlap area in these metal–insulator–metal (MIM) capacitors is 150 × 150 μm (1, black), 250 × 250 μm (2, red), 400 × 400 μm (3, blue), and 550 × 550 μm (4, green). d) SEM and microscope images (inset) of planar spiral coils on a Mo foil substrate (≈10 μm) (left). Mg layers provide bottom (≈300 nm) and top (≈3.5 μm) electrodes, and a PECVD SiO_2 layer (≈900 nm) serves as interlayer dielectric. Inductance as a function of frequency from 0 to 15 GHz (right). The number of turns (*n*), outer diameter (*d*), and metal width/space (*w*/*s*) of these spiral coils are 3, 440 μm, 20/20 μm (1, black); 2, 440 μm, 40/20 μm (2, red); 2, 1 mm, 100/20 μm (3, blue); 3, 1 mm, 50/20 μm (4, green).

of security systems and environmentally sustainable devices, where alternative approaches based on organic materials and polymers might not be suitable) and in scenarios that involve magnetic positioning (for implantable devices that require precise, noninvasive remotely controlled placement).[21,22]

Direct fabrication procedures like those described above can yield many classes of components. **Figure 2**a,b provides scanning electron microscope (SEM) images of an array of transistors and diodes, respectively, with magnified views in the inset (left), and electrical properties (right). Each *n*-channel MOSFET

© 2015 WILEY-VCH Verlag GmbH & Co. KGaA, Weinheim

shown here consists of a doped Si NM (≈300 nm, active layer), a layer of PECVD SiO_2 (≈100 nm, gate dielectric), Mg electrodes (≈300 nm, source/drain/gate contacts) on Fe or W substrates (see Figure S2, Supporting Information, for W substrate), with channel length and width of ≈30 and ≈600 μm, respectively. Current–voltage characteristics of a representative device measured at different gate biases appear in the right frame of Figure 2a. Figure 2b shows an image of an array of PIN diodes (left), each of which consists of a doped Si NM (≈200 nm) with Mg electrodes (≈300 nm) on a Zn foil (≈10 μm), and typical electrical characteristics (right).

Capacitors (Figure 2c) and inductors (Figure 2d) are also possible. Parallel-plate capacitors of various lateral dimensions (left, black, 150 × 150 μm; red, 250 × 250 μm; blue, 400 × 400 μm; green, 550 × 550 μm) can be formed with SiO_2 (≈900 nm) as the dielectric and Mg as the electrodes on Mo foils (≈10 μm). Capacitances (Figure 2c, right) and unloaded Q factors (Figure S3a, Supporting Information) in the frequency range between 0 and 25 GHz exhibit trends and values comparable to those of otherwise similar devices on biodegradable polymer substrates.[12] Spiral inductors with two or three turns (Figure 2d, left) constructed using Mg traces for the electrodes and SiO_2 (≈900 nm) as the interlayer dielectric can be formed on Mo foils (≈10 um). The resonance frequencies and unloaded Q factors (Figure 2d, right; Figure S3b, Supporting Information) have values that differ from those of devices on polymers,[12] likely due to parasitics associated with the conductive substrate. Such effects can be minimized either by reducing the capacitance of the insulating layer (e.g., increasing its thickness and decreasing its dielectric constant) or by employing ground shielding layers and other advanced device structures.[23,24]

Previous studies explored dissolution behaviors of degradable metals (Mg, Mo, Zn, Fe, and W) in the form of thin films.[6,25–28] Since the thickness, grain structure, and surface morphology can potentially dictate the kinetics of hydrolysis,[6] related studies of metal foils are necessary. **Figure 3**a presents a series of images of transient *n*-MOSFETs on a Mo foil (≈5 μm) at various times for partial immersion in phosphate buffer solution (PBS, pH 7.4, Sigma-Aldrich, USA) at 90 °C. Complete dissolution of the foil occurs after 25 days under these conditions; the other materials dissolve at different rates, as reported elsewhere.[4,7–9] Dissolution can proceed by through the materials themselves and along the interfaces between the different layers. In general, large scale failures in adhesion and associated release of large pieces of material are uncommon. The regions of Mg directly adjacent to the water undergo partial dissolution due to the combined effects of wetting by the water and exposure to water vapor. Figure 3b shows additional details on related behaviors for the other metal foils. The changes in film thickness in PBS (pH 7.4 at 37 °C) are 0.02, 3.5, 0.08, and 0.15 μm day^{-1} for Mo, Zn, Fe, and W, respectively. The dissolution rates of thin films of these metals in Hanks' solution at 37 °C are 0.005, 7.2, 0.005, and 0.19 μm day^{-1}.[6] For Zn and W, metal foils in PBS dissolved faster than thin films in Hanks' solution. Metal foils of Mo and Fe, on the other hand, dissolved slower in PBS than corresponding thin films in Hanks' solution. These varied results likely follow from the effects of morphology of metal foils and thin films, as well as different ionic content and concentrations of solutions.[6,9] Figure 3c shows thickness profiles of Mo foils during the dissolution tests; the metal foils disappear in a uniform fashion without significant changes in surface morphology.

Spin-on glass offers attractive properties as an adhesive interlayer in these systems due to its ability to form uniform, conformal coatings.[29–32] Established use in conventional electronics and an ability to select its properties by appropriate chemical design further motivate the use of such materials for encapsulants and dielectric layers. The dissolution behaviors of silicate-based spin-on glass (hydrogen silsesquioxane, HSQ) cured under different conditions are thus important. Figure 3d shows the kinetics of hydrolysis of spin-on glass cured at different temperatures (300, 400, and 800 °C) after immersion in PBS (pH 7.4) at 37 °C. SOG cured at 300 °C dissolves faster (≈50 nm day^{-1}) than that cured at 800 °C (≈6 nm day^{-1}) at nitrogen environment. The curing reaction is based on high-temperature condensation between $Si(OH)_4$ molecules to yield H_2O and Si–O–Si bonds, with a resulting volumetric shrinkage as described in Figure S4, Supporting Information.[29–32] The extent of this reaction varies depending on the curing temperature and time; the unreacted parts remain as Si–OH.[29–32] Consequently, spin-on glass cured at lower temperature (300 °C) has highest Si–OH content[29–32] and fastest rates of hydrolysis than those cured at higher temperatures (400 and 800 °C). Fourier-transform infrared spectroscopy (FTIR) reveals the dependence of —OH content of the spin-on glass prepared at three different curing temperatures (Figure 3e). The stretching modes between 3600 and 3200 cm^{-1},[29,31] which reflect the –OH content, show that the spin-on glass cured at 300 °C has more –OH than that at 800 °C, demonstrating the tunability of the dissolution rate through control of curing temperatures. Surface topography measurements on SOG materials cured at three different temperatures appear in Figure S5, Supporting Information.

Figure 4 summarizes the effects of transience by hydrolysis on the electrical function of devices on metal foils. Systems in geometries similar to those of Figure 2, but with extended electrodes (see insets in Figure 4a,b), allow remote measurements while immersed in deionized (DI) water at room temperature. Figure 4a illustrates transfer curves of Si *n*-MOSFETs at V_d = 0.1 V (left), and drain current (I_d, right) at V_g = 5 V. The data indicate stable operation for ≈5 h, followed by rapid loss of function due to dissolution of the Mg electrodes. Measurements on transient Si PIN diodes show similar behaviors, as shown in Figure 4b. The transient capacitors and inductors evaluated at 10 MHz appear in Figure 4c,d. Here, different thicknesses of a MgO encapsulation layer provide two-stage kinetics: the first stage (stable operation) is defined by dissolution and/or permeability of the encapsulants (e.g., MgO in this case); the second stage (rapid degradation) is determined by hydrolysis of device materials (mainly the Mg electrodes). The first time period can be adjusted by choice of thickness and composition of encapsulants.

Envisioned applications in biomedicine motivate in vitro and in vivo evaluations of biocompatibility/toxicity of SOG. Dissolvable metals, such as Mg, Fe, and Zn, have been extensively used in degradable intravascular stents due to their excellent biocompatibility,[1,28,33–35] and use of W as embolization coils revealed no obvious harmful effects.[36,37] Mo is classified as an essential element with recommended daily intake of 0.1–0.5 mg.[38] Studies presented here involve a metastatic breast cancer cell line

© 2015 WILEY-VCH Verlag GmbH & Co. KGaA, Weinheim

DOI: 10.1002/adfm.201403469

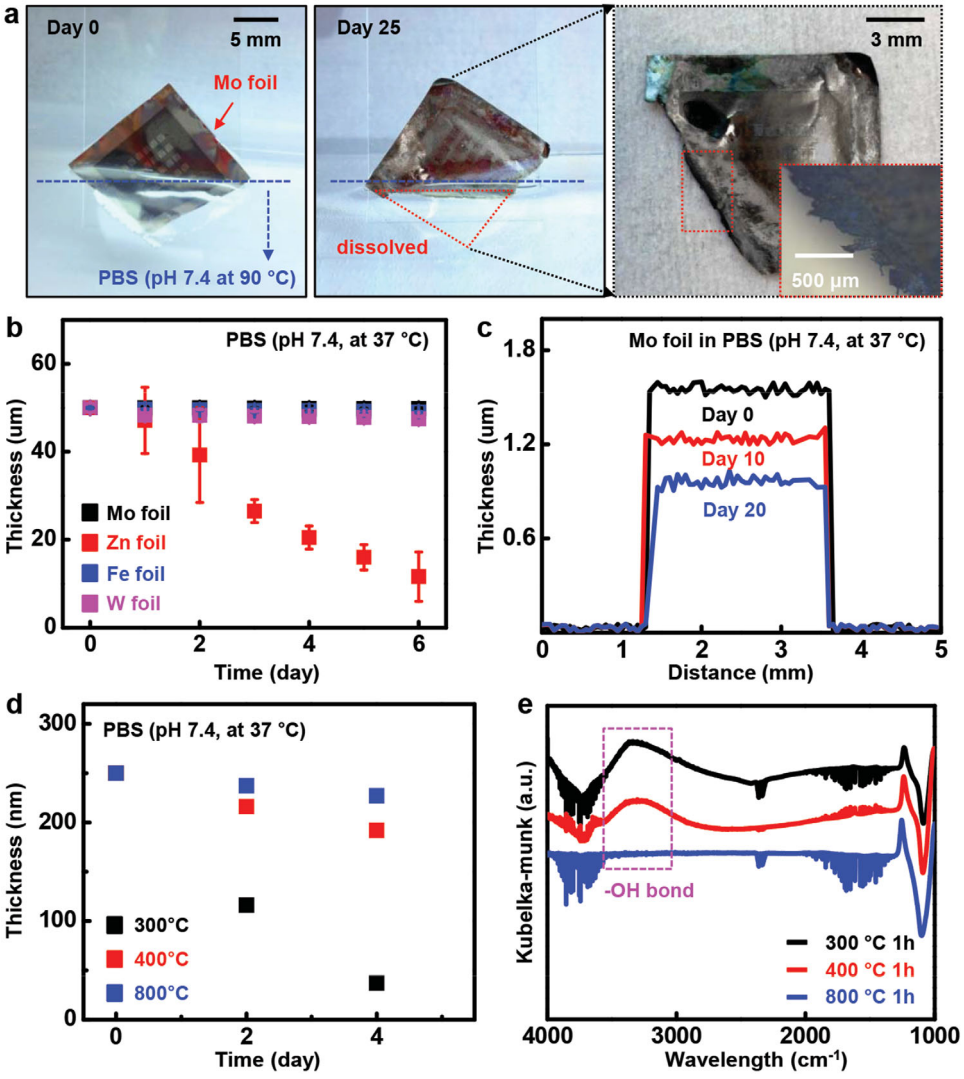

Figure 3. Dissolution of various metal foils and spin-on glass. a) Sequential images collected at various stages of dissolution of a transistor array on a Mo foil (≈5 μm) partially immersed in phosphate buffer solution (PBS, pH 7.4) at 90 °C. The device in its initial state (left) and partially dissolved after 25 days (middle). Magnified (right) and microscope (inset) images show full dissolution in immersed areas and partial degradation of Mg electrodes by vapor in an adjacent region. b) Measured dissolution kinetics of metal foils (initial thickness ≈50 μm) in PBS (pH 7.4) at 37 °C (black, Mo; red, Zn; blue, Fe; magenta, W). c) Line scan profiles of changes in thickness of a Mo foil under the same conditions (black, after 0 day; red, 10 days; blue, 20 days). d) Measured dissolution rates of spin-on glass (SOG) cured at different temperatures in PBS solution (pH 7.4) at physiological temperature (37 °C) (black, 300; red, 400; blue, 800 °C; cured for 1 h). e) Chemical structure of SOG cured at various temperatures, observed by Fourier-transform infrared spectroscopy (FTIR) (black, 300; red, 400; blue, 800 °C; cured for 1 h). The concentration of the hydroxide groups decreases as the curing temperature increases.

(MDA-MB-231) seeded and cultured on a substrate of SOG patterned into an array of dots (3 μm × 3 μm × 250 nm) on thermal oxide on Si. The breast cancer cell line is attractive for present purposes due to its rapid propagation and culture, as in previously reported studies of Si nanomembranes.[9] Two types of SOG, cured at 300 and 800 °C for 1 h, reveal the effects of degree of curing on biocompatibility. A PDMS well placed on the SOG chip forms a microincubation chamber for an extended culture environment. Sterilizing and sealing the patterned SOG sample in the PDMS chamber, allows cells to be cultured and imaged for nine days. **Figure 5**a,b shows the growth and proliferation behaviors of cells on the two different SOG samples. Differential interference contrast (DIC) images reveal that SOG dot arrays completely dissolve after three and nine days for samples cured at 300 and 800 °C, respectively. Daily measurements of the thickness of the SOG performed on separate samples following removal of the cells at each stage using trypsin appear in Figure 5c. A fluorescence-based live/dead assay revealed cell viability on days 1, 3, 6, and 9, as depicted by a set of fluorescent images. Figure 5d shows the numbers of live (green) and dead (red) cells. Overall, cell viability for both types of SOG range from 0.92 to 0.95, indicating that the SOG as well as products of its dissolution are not toxic. The results suggest, indirectly, that the Si–OH content does not significantly affect biocompatibility of SOG materials. Details of the cell culture procedure appear in the Experimental Section. Examination using other cell lines represents a direction of current work.

© 2015 WILEY-VCH Verlag GmbH & Co. KGaA, Weinheim

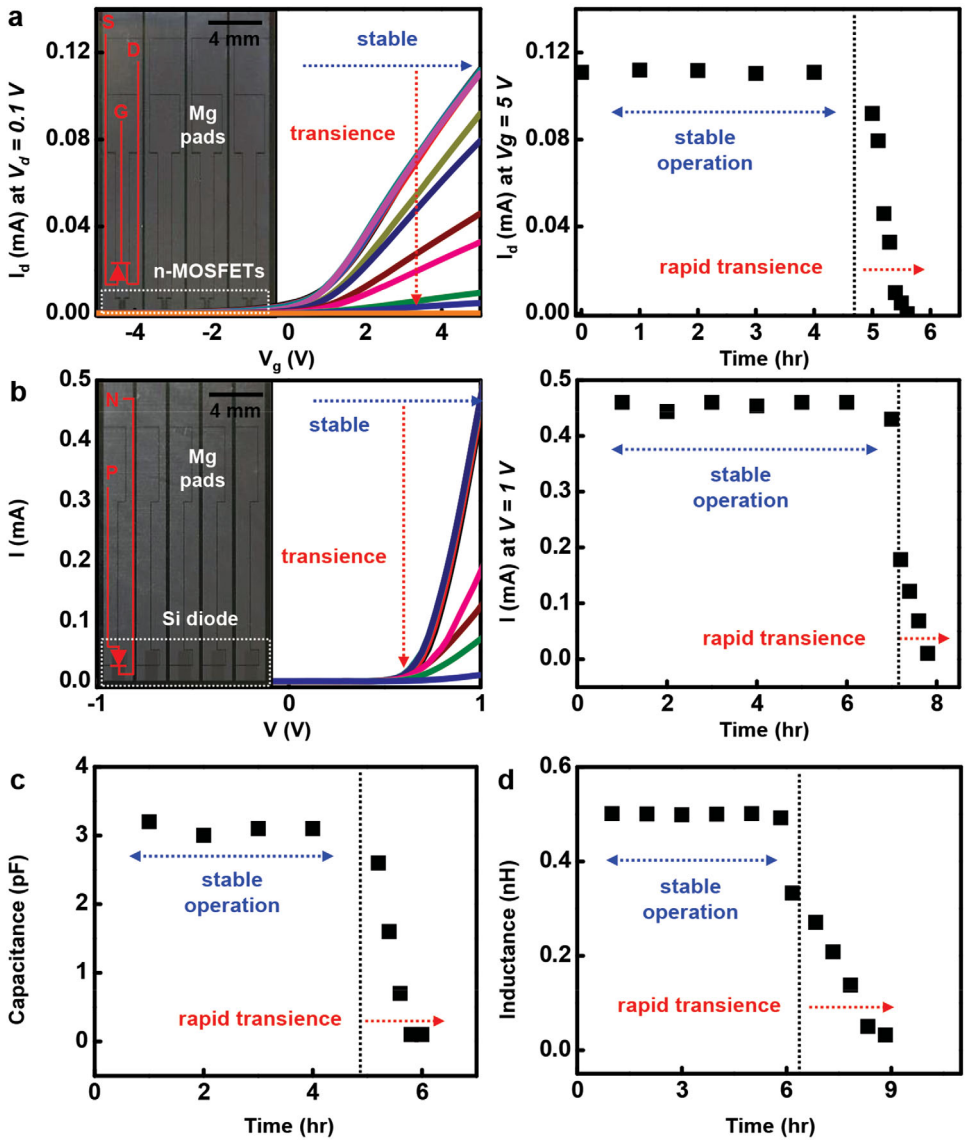

Figure 4. Measurements of transience at the device level. a) Measured drain currents (at $V_d = 0.1$ V) of typical *n*-MOSFET (left); image in the inset. The drain current I_d at $V_g = 5$ V as a function of time (right). The different colored curves (left) indicate responses at different times, where corresponding current values at $V_g = 5$ V appear in separate plots (right). b) Changes in current in a Si PIN diode (left; image of device in inset). Measured current changes (at $V = 1$ V) as a function of time (right). The different colored curves of left side graph are measured at different time intervals corresponding to one of right side graph. c) Measured capacitance of a MIM capacitor as a function of time. d) Measured degradation in inductance of a Mg spiral inductor. In all cases, the systems were encapsulated in MgO (1–3 μm) and immersed in DI water at room temperature. The transience shows two-stage kinetics involving stable operation for several hours, followed by rapid degradation. The encapsulation layers and the Mg electrodes define the first and second time frames, respectively.

3. Conclusion

The results presented here demonstrate that degradable metal foils can be used as substrates for active and passive electronic systems in which all components and constituent materials are biodegradable and biocompatible. Foils have significant advantages over previously explored organic polymer substrates, including capabilities for direct (on-substrate) device fabrication, high-temperature stability, hermeticity, and absence of swelling. In this context, spin-on glass is an attractive choice as a planarization and electrical insulation layer, to isolate the foils from the electronics. These findings provide important design options in transient electronics.

4. Experimental Section

Fabrication of Transient Electronics (n-Channel Silicon MOSFETs, Si Pin Diodes, Capacitors, and Inductors) on Dissolvable Metal Substrates: Fabrication began with laminating iron (Fe), molybdenum (Mo), tungsten (W), and zinc (Zn) foils (≈10 μm thick; Goodfellow, USA) on PDMS (Dow Corning, USA) coated on glass slides to facilitate processing. PECVD formed layers of SiO_2 (≈1 μm) on these foils for

© 2015 WILEY-VCH Verlag GmbH & Co. KGaA, Weinheim
Adv. Funct. Mater. **2015**,
DOI: 10.1002/adfm.201403469

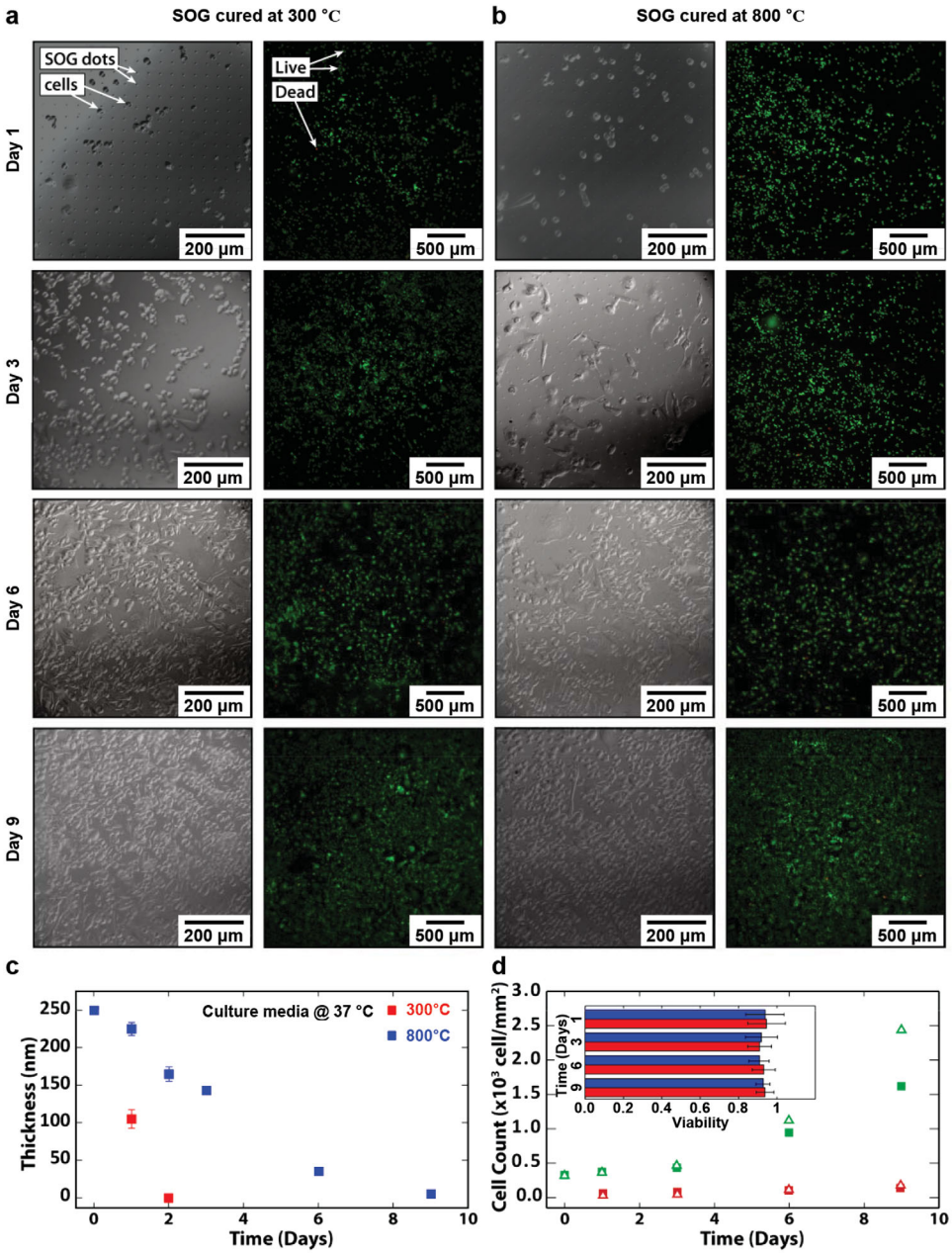

Figure 5. In vitro cell culture evaluations of dissolution and cytotoxicity of silicate spin-on glass. a) A set of differential interference contrast images (left) and fluorescent images (right) showing the dissolution behaviors and cell viability of SOG cured at 300 °C and b) SOG cured at 800 °C. Living cells appear green, and dead cells appear red. c) Change in thickness of spin-on glass dissolved in cell culture media (red, SOG cured at 300 °C; blue, SOG cured at 800 °C). d) Numbers of both live (green) and dead (red) cells over time as quantified from the live/dead assay (solid squares, SOG cured at 300 °C; open triangles, SOG cured at 800 °C). Inset: Cell viability over 1, 3, 6, and 9 days, calculated as the fraction of total living cells (red line, SOG cured at 300 °C; blue line, SOG cured at 800 °C).

electrical isolation. Silicon-on-insulator (SOI) wafers (SOITEC, France) served as a source of Si NM; solid-state phosphorus and boron doping occurred at 950 and 1000 °C, respectively, to define active regions for transistors and diodes. Removal of the buried oxide of the SOI substrates by hydrofluoric acid (HF), allowed transfer printing of the Si NMs onto a thin layer of silicate SOG (Filmtronics, Inc., USA) cast on the PECVD SiO_2-coated foils. Curing of the SOG for the device examples occurred at 300 °C for 1 h. RIE (Plasmatherm, USA) with SF_6 gas through a photopatterned layer of resist S1805 (Microchem, USA) defined the top device layers. For the *n*-channel MOSFET, PECVD SiO_2 (≈100 nm) served as a gate dielectric, and etching with buffered oxide etchant (6:1, BOE, Transene Company, Inc., USA) defined openings for source and drain contacts. A lift-off process with photoresist AZ2070 (Microchem, USA) and electron-beam (E-beam) evaporation yielded Mg (≈300 nm) electrodes.

Similar lift-off procedures define the bottom electrodes for both capacitors and inductors (Mg, ≈300 nm). A layer of PECVD SiO_2 (≈900 nm) formed the interlayer dielectrics. A thick layer of Mg (≈3.5 μm) defined the top contacts. Immersion in pentane for ≈2 h released the completed devices from the underlying PDMS.

RF Characterizations of Devices: The scattering- (s-) parameters for spiral inductors and MIM capacitors were measured using an Agilent

© 2015 WILEY-VCH Verlag GmbH & Co. KGaA, Weinheim

E8364A network analyzer (45 MHz–25 GHz). The system was calibrated to the probe tips using a standard Short-Open-Load-Thru (SOLT) on-wafer probing kit for a frequency range of 45 MHz–25 GHz. The critical passive component parameters, such as inductance/capacitance (L/C) values, quality (Q) factor, and resonant frequency values, were extracted from measured s-parameters using Agilent Advanced Design System (ADS). To extract the L, C, and Q-factor values, the measured *s*-parameter was converted to *y*-parameter using Equations (1)–(5)

$$D = [(1+S(1,1)) \times (1+S(2,2)) - [S(1,2) \times S(2,1)] \quad (1)$$

$$Y(1,1) = [(1-S(1,1)) \times (1+S(2,2)) + S(1,2) \times S(2,1)] / D \quad (2)$$

$$Y(1,2) = -2 \times S(1,2) / D \quad (3)$$

$$Y(2,1) = -2 \times S(2,1) / D \quad (4)$$

$$Y(2,2) = [(1+S(1,1)) \times (1-S(2,2)) + S(1,2) \times S(2,1)] / D \quad (5)$$

Then, extract the *L*, *C*, and *Q*-factor values using Equations (6)–(8)

$$L = \frac{\mathrm{Im}\left(\frac{1}{Y_{11}}\right)}{\omega} \quad (6)$$

$$L = \frac{\mathrm{Im}(Y_{11})}{\omega} \quad (7)$$

$$Q = \frac{\mathrm{Im}(Y_{11})}{\mathrm{Re}(Y_{11})} \quad (8)$$

Dissolution Tests of Metal Foils and Spin-On Glass: Dissolution tests on metal foils (Fe, Mo, Zn, and W foils, ≈10 μm) and silicate-based spin-on glass (cast on Si wafer and cured at 300, 400, and 800 °C for 1 h) involved placing each sample into 50 mL of PBS (pH 7.4, Sigma-Aldrich, USA) at 37 °C. Removing the samples from the solution and rinsing them in DI water allowed measurement of their thicknesses by profilometry (Dektak 3030, Sloan Technology Co., USA) for metal foils and by spectroscopic ellipsometry (J. A. Wooldman Co., Inc., USA) for SOG. FTIR (Thermo Nicolet Nexus 670, USA) in diffuse reflection mode revealed the hydroxide composition of the SOG. After measurement, the samples were reimmersed in fresh solutions. The solutions were replaced every other day.

Cell Culture Experiments: The microincubation culture chamber consisted of a 100 μL PDMS well made by creating a hole with a 6 mm dermal punch through a 4 mm thick piece of PDMS, subsequently attached directly to each chip. Rinsing with 80% ethanol sterilized the chip and culture chamber prior to cell seeding. Highly metastatic human breast adenocarcinoma cells (MDA-MB-231 ATCC # HTB-26) were cultured in Leibovitz's L-15 Medium (Sigma-Aldrich) with 10% fetal bovine serum and 1% penicillin streptomycin. Treatments with 0.25% trypsin–EDTA (Gibco) detached the cells from a T-25 flask. Adding 3–5 mL of growth medium neutralized the trypsin–EDTA and cell suspension, allowing separation by centrifugation at 200 rcf for 6 min, followed by resuspending in fresh growth medium, diluted to proper to a density of 300 cells mm^{-2}, and seeding into the microincubation chamber on the chip. After a cell settling time of 15 min, the PDMS chamber was hermetically and reversibly sealed with a coverslip, presterilized with 70% ethanol. The cells were incubated at 37 °C for extended periods and then removed at 1, 3, 6, and 9 days to allow measurement of the thickness of SOG by AFM (MFP-3D AFM, Asylum Research, USA). An immunofluorescence live/dead assay (Invitrogen, Carlsbad, CA) allowed testing for cell viability after extended on-chip culture. Tested samples with adhered cells were incubated with 1×10^{-6} M calcein AM (green; live) and 2×10^{-6} M of ethidium homodimer (red; dead) for 35 min in PBS. The cells were then rinsed twice with PBS and the samples were immediately imaged. Viable and dead cells appeared through green and red fluorescence, respectively. ImageJ enabled counting and calculating the densities of cells in the FITC (green; live) and the TRITC (red; dead) channels. The ratio of integrated density in the FITC to TRITC channel corresponds to the reported cell viability.

Study of Functional Transience at the Device Level: Mo foils (≈10 μm) served as substrates for transient active and passive components. Layers of MgO (≈1 μm for transistors and diodes, and ≈3 μm for capacitors and inductors) encapsulated the devices, except at contact pads for probing electrical properties. The devices were partially immersed in DI water at room temperature during electrical measurements.

Supporting Information

Supporting Information is available from the Wiley Online Library or from the author.

Acknowledgements

S.-K.K. and S.-W.H. contributed equally to this work. This material is based upon work supported by the Defense Advanced Research Projects Agency.

Received: October 4, 2014
Revised: November 28, 2014
Published online:

[1] P. P. Mueller, S. Arnold, M. Badar, D. Bormann, F.-W. Bach, A. Drynda, A. Meyer-Lindenberg, H. Hauser, M. Peuster, *J. Biomed. Mater. Res. A* **2012**, *100A*, 2881.
[2] Z. Li, X. Gu, S. Lou, Y. Zheng, *Biomaterials* **2008**, *29*, 1329.
[3] N. Erdmann, N. Angrisani, J. Reifenrath, A. Lucas, F. Thorey, D. Bormann, A. Meyer-Lindenberg, *Acta Biomater.* **2011**, *7*, 1421.
[4] S.-W. Hwang, H. Tao, D.-H. Kim, H. Cheng, J.-K. Song, E. Rill, M. A. Brenckle, B. Panilaitis, S. M. Won, Y.-S. Kim, Y. M. Song, K. J. Yu, A. Ameen, R. Li, Y. Su, M. Yang, D. L. Kaplan, M. R. Zakin, M. J. Slepian, Y. Huang, F. G. Omenetto, J. A. Rogers, *Science* **2012**, *337*, 1640.
[5] C. Dagdeviren, S.-W. Hwang, Y. Su, S. Kim, H. Cheng, O. Gur, R. Haney, F. G. Omenetto, Y. Huang, J. A. Rogers, *Small* **2013**, *9*, 3398.
[6] L. Yin, H. Cheng, S. Mao, R. Haasch, Y. Liu, X. Xie, S.-W. Hwang, H. Jain, S.-K. Kang, Y. Su, R. Li, Y. Huang, J. A. Rogers, *Adv. Funct. Mater.* **2014**, *24*, 645.
[7] S.-W. Hwang, G. Park, H. Cheng, J.-K. Song, S.-K. Kang, L. Yin, J.-H. Kim, F. G. Omenetto, Y. Huang, K.-M. Lee, J. A. Rogers, *Adv. Mater.* **2014**, *26*, 1992.
[8] S.-K. Kang, S.-W. Hwang, H. Cheng, S. Yu, B. H. Kim, J.-H. Kim, Y. Huang, J. A. Rogers, *Adv. Funct. Mater.* **2014**, *24*, 4427.
[9] S.-W. Hwang, G. Park, C. Edwards, E. A. Corbin, S.-K. Kang, H. Cheng, J.-K. Song, J.-H. Kim, S. Yu, J. Ng, J. E. Lee, J. Kim, C. Yee, B. Bhaduri, Y. Su, F. G. Omennetto, Y. Huang, R. Bashir, L. Goddard, G. Popescu, K.-M. Lee, J. A. Rogers, *ACS Nano* **2014**, *8*, 5843.
[10] S.-W. Hwang, J.-K. Song, X. Huang, H. Cheng, S.-K. Kang, B. H. Kim, J.-H. Kim, S. Yu, Y. Huang, J. A. Rogers, *Adv. Mater.* **2014**, *26*, 3905.
[11] S.-W. Hwang, D.-H. Kim, H. Tao, T.-I. Kim, S. Kim, K. J. Yu, B. Panilaitis, J.-W. Jeong, J.-K. Song, F. G. Omenetto, J. A. Rogers, *Adv. Funct. Mater.* **2013**, *23*, 4087.
[12] S.-W. Hwang, X. Huang, J.-H. Seo, J.-K. Song, S. Kim, S. Hage-Ali, H.-J. Chung, H. Tao, F. G. Omenetto, Z. Ma, J. A. Rogers, *Adv. Mater.* **2013**, *25*, 3526.

© 2015 WILEY-VCH Verlag GmbH & Co. KGaA, Weinheim

[13] H. Acar, S. Çınar, M. Thunga, M. R. Kessler, N. Hashemi, R. Montazami, *Adv. Funct. Mater.* **2014**, *24*, 4135.
[14] M. Irimia-Vladu, P. A. Troshin, M. Reisinger, L. Shmygleva, Y. Kanbur, G. Schwabegger, M. Bodea, R. Schwödiauer, A. Mumyatov, J. W. Fergus, V. F. Razumov, H. Sitter, N. S. Sariciftci, S. Bauer, *Adv. Funct. Mater.* **2010**, *20*, 4069.
[15] M. Irimia-Vladu, E. D. Głowacki, G. Voss, S. Bauer, N. S. Sariciftci, *Mater. Today* **2012**, *15*, 340.
[16] M. Irimia-Vladu, *Chem. Soc. Rev.* **2013**, *43*, 588.
[17] P. Meredith, C. J. Bettinger, M. Irimia-Vladu, A. B. Mostert, P. E. Schwenn, *Rep. Prog. Phys.* **2013**, *76*, 034501.
[18] C. J. Bettinger, Z. Bao, *Adv. Mater.* **2010**, *22*, 651.
[19] C. J. Bettinger, Z. Bao, *Polym. Int.* **2010**, *59*, 563.
[20] L. D. Landau, E. M. Lifshitz, *Theory of Elasticity*, Butterworth-Heinemann, NJ, USA **1987**.
[21] S. Kim, F. Qiu, S. Kim, A. Ghanbari, C. Moon, L. Zhang, B. J. Nelson, H. Choi, *Adv. Mater.* **2013**, *25*, 5863.
[22] B. Ozkale, E. Pellicer, A. M. Zeeshan, J. F. Lopez-Barbera, J. Nogues, J. Sort, B. J. Nelson, S. Pane, *Nanoscale* **2014**, *6*, 4683.
[23] C. P. Yue, S. Wong, at ACM 36th Design Automation Conference, NY, USA, **1999**, p. 982.
[24] M. Raieszadeh, P. Monajemi, S. W. Yoon, J. Laskar, F. Ayazi, at 18th IEEE Micro Electro Mechanical Systems Conference, FL, USA **2005**, p. 199.
[25] N. T. Kirkland, N. Birbilis, M. P. Staiger, *Acta Biomater.* **2012**, *8*, 925.
[26] E. Patrick, M. E. Orazem, J. C. Sanchez, T. Nishida, *J. Neurosci. Methods* **2011**, *198*, 158.
[27] W. A. Badawy, F. M. Al-Kharafi, *Electrochim. Acta* **1998**, *44*, 693.
[28] P. K. Bowen, J. Drelich, J. Goldman, *Adv. Mater.* **2013**, *14*, 2577.
[29] M. Speciale, C. L. Rosa, D. Grasso, A. Porto, P. Lanza, C. Magro, *Mater. Res. Soc. Symp. Proc.* **1991**, *204*, 539.
[30] Y. Nishi, R. Doering, *Handbook of Semiconductor Manufacturing Technology*, Marcel Dekker, NY **2000**.
[31] N. Iwamoto, M. M. F. Yuen, H. Fan, *Molecular Modeling and Multi-scaling Issues for Electronic Material Applications*, Springer, New York **2012**.
[32] N. N. Toan, *Spin-on Glass Materials and Applications in Advanced IC Technologies*, University of Twente, AE Enschede, Netherlands **1999**.
[33] H. Hermawan, A. Purnama, D. Dube, J. Couet, D. Mantovani, *Acta Biomater.* **2010**, *6*, 1852.
[34] R. Zeng, W. Dietzel, F. Witte, N. Hort, C. Blawert, *Adv. Eng. Mater.* **2008**, *10*, B3.
[35] F. Witte, *Acta Biomater.* **2010**, *6*, 1680.
[36] M. Peuster, C. Fink, C. von Schnakenburg, *Biomaterials* **2003**, *24*, 4057.
[37] N. Strigul, *Ecotoxicol. Environ. Safety* **2010**, *73*, 1099.
[38] D. G. Barceloux, *J. Toxicol.: Clin. Toxicol.* **1999**, *37*, 231.

© 2015 WILEY-VCH Verlag GmbH & Co. KGaA, Weinheim